

Characterizing the Palomar 5 Stream: HDBSCAN Analysis and Galactic Halo Constraints

Yun-Ao Xiao^{1,2}, Hu Zou^{1,2}, Lu Feng¹, Wei-Jian Guo¹, Niu Li¹, Wen-Xiong Li¹, Shu-Fei Liu^{1,2}, Gaurav Singh¹, Ji-Peng Sui^{1,2}, Jia-Li Wang¹ and Sui-Jian Xue¹

¹ National Astronomical Observatories, Chinese Academy of Sciences, Beijing 100012, China;
zouhu@nao.cas.cn

² University of Chinese Academy of Sciences, Beijing 100039, P.R. China

Received 20xx month day; accepted 20xx month day

Abstract We utilize the DESI Legacy Imaging Surveys DR10 to investigate the previously undetected faint extension of the Palomar 5 stellar stream. By applying the HDBSCAN clustering algorithm, we identify stream members and successfully extend the leading arm of the stream to approximately $\text{DEC} \sim -15^\circ$. Combining the fully detected stream with a suite of mock stream simulations, we conduct a detailed comparison to constrain both the intrinsic properties of the stream and the dynamical parameters of the Milky Way (MW) halo. Our analysis yields a best-fit model characterized by eight parameters: $M_{\text{halo}} = 5.67 \times 10^{11} M_\odot$, $r_{s,\text{halo}} = 28.94 \text{ kpc}$, $q_z = 0.93$, $M_{\text{gc}} = 4.31 \times 10^3 M_\odot$, $dM_{\text{gc}}/dt = 1.81 M_\odot \text{ Myr}^{-1}$, $\mu_\alpha \cos \delta = -2.28 \text{ mas yr}^{-1}$, $\mu_\delta = -2.26 \text{ mas yr}^{-1}$, and $D = 23.25 \text{ kpc}$. Notably, our constraints on the halo shape indicate that the MW's dark matter halo exhibits a flattened potential, with a minor-to-major axis ratio of $q_z = 0.93$. This finding aligns well with theoretical expectations and previous observational estimates. Additionally, the best-fit model accurately reproduces the observed stream morphology and dynamics, providing a more precise understanding of both the evolution of the stream and the overall structure of the Galactic halo.

Key words: Galaxy: halo – Galaxy: kinematics and dynamics – Galaxy: structure – globular clusters: individual (Palomar 5)

1 INTRODUCTION

Due to their longevity and coherence, tidal streams have become essential probes for testing models of the Galactic potential. Subtle features such as gaps, bifurcations, or density variations often observed in these streams may arise from interactions with dark matter subhalos or baryonic perturbers, including molecular

2019). Within the framework of the Λ CDM standard cosmology, these features provide direct observational tests of the predicted population of low-mass dark matter subhalos that do not host luminous galaxies. The detection of such substructures serves as a crucial test of Λ CDM and aids in distinguishing it from alternative dark matter models or modified gravity theories (Bode & et al. 2001; Milgrom 1983; Kroupa 2015). Observational efforts, such as those by Price-Whelan & Bonaca (2018) and Bonaca & Hogg (2018), have revealed gaps and spurs in streams like GD-1, which may reflect perturbations from unseen dark matter subhalos (Bonaca et al. 2019). These findings underscore the potential of stellar streams to test the Λ CDM paradigm and investigate the detailed structure of the Galactic halo.

The discovery and characterization of tidal streams have accelerated in recent years, driven by deep, wide-field photometric and astrometric surveys such as SDSS, Pan-STARRS, DES, and Gaia. In particular, Gaia’s high-precision astrometry has revolutionized the study of stellar streams by enabling the identification of member stars with unprecedented accuracy. These surveys have provided comprehensive measurements of stellar populations, proper motions, and distances, facilitating detailed mapping of stream morphologies and kinematics (Koposov & et al. 2010; Küpper & et al. 2015; Bovy & Rix 2016; Ibata et al. 2024; Bonaca & Price-Whelan 2024). Consequently, stellar streams have become critical tools for constraining the shape, orientation, and mass profile of the Milky Way (MW) halo, as well as reconstructing its accretion history. Additionally, tidal streams have been the focus of extensive dynamical and chemical investigations. Dynamical modeling has enabled the reconstruction of progenitor orbits and the underlying Galactic potential, while spectroscopic and photometric analyses of stream stars have revealed the chemical signatures of their progenitors and the evolutionary history of the halo (Carlberg & et al. 2012; Bernard & et al. 2016; Ibata & et al. 2016; Thomas & et al. 2016; Erkal & et al. 2017). Together, these complementary approaches have significantly enhanced our understanding of stream formation and the hierarchical build-up of the MW.

Among the known streams, the Palomar 5 stream is one of the most prominent and well-studied examples. First discovered by Odenkirchen & et al. (2001) and further characterized by Rockosi & et al. (2002), it was initially observed as a narrow, low-surface-brightness structure extending from the Palomar 5 globular cluster. Subsequent observations using deeper imaging surveys, such as SDSS (Bernard & et al. 2016) and the DESI Legacy Survey (Bonaca et al. 2020), have uncovered the extended trailing and leading tails of the stream, enabling its detection across a wide region of the sky. Due to its well-defined morphology and relatively low internal dispersion, the Palomar 5 stream has been extensively used to constrain the shape and mass distribution of the MW dark matter halo (Carlberg & et al. 2012; Pearson et al. 2015). Several studies have explored the response of the stream to both dark matter and baryonic perturbations, including the effects of the Galactic bar and molecular clouds (Pearson & D’Onghia 2017; Amorisco et al. 2016). These analyses have provided compelling evidence for a dark matter halo that is near-spherical or mildly flattened, consistent with predictions from the Λ CDM cosmology.

Detecting the outer regions of the Palomar 5 stream has been challenging due to the limitations in the depth and sky coverage of earlier surveys. While SDSS and Pan-STARRS provide valuable data, they are typically too shallow to fully capture the faint outskirts of the stream (Bernard & et al. 2016; Ibata &

its dynamical interaction with the Galactic halo remain poorly characterized. The DESI Legacy Imaging Surveys DR10 offers deeper and broader photometric coverage than previous datasets. This allows us to detect fainter stream members and accurately trace the outermost regions of the Palomar 5 stream. In this work, we aim to construct a more comprehensive morphological map of the stream, investigate its dynamical evolution under various Galactic potential models, and explore the effects of both baryonic and dark matter perturbations.

The structure of this paper is organized as follows. In Section 2, we describe the observational data used for detecting the tidal stream of Palomar 5. Section 3 outlines the methodology employed in identifying stream members and construct the updated stream map. Section 4 details the generation of mock streams for model comparison. In Section 5, we present our results and compare the observed stream to simulations. Finally, Sections 5.3 and 6 discuss our findings and summarize our conclusions, respectively.

2 PHOTOMETRIC DATA AND SELECTION OF CLUSTER MEMBERS

2.1 DESI Legacy Imaging Surveys

The DESI Legacy Surveys represent a coordinated effort to construct a multi-wavelength inference model of the extragalactic sky, combining optical and infrared imaging to support large-scale spectroscopic studies. Initially, the project focused on three dedicated northern hemisphere surveys, including Beijing-Arizona Sky Survey (BASS; Zou et al. 2017), DECam Legacy Survey (DECaLS; Blum et al. 2016), and Mayall z -band Legacy Survey (MzLS; Silva et al. 2016), which collectively mapped $\sim 14,000$ square degrees in the g , r , and z optical bands. These datasets were complemented by four mid-infrared bands (W1–W4) from the NEOWISE mission (Wright et al. 2010; Mainzer et al. 2014), enabling cross-wavelength source characterization. The foundational surveys established a photometric backbone for spectroscopic target selections of the DESI project (DESI Collaboration et al. 2016). Data processing follows a two-stage pipeline as detailed in Dey et al. (2019): raw images are first reduced via the NOIRLab Community Pipeline for basic calibration, then refined using the Legacypipe software to homogenize photometry, remove artifacts, and generate co-added sky maps. Infrared counterparts are anchored through forced photometry on unWISE maps, incorporating seven years of NEOWISE-Reactivation data to extract WISE fluxes at optical source positions.

With Data Release 10 (DR10), the Legacy Surveys have significantly expanded their scope, now covering over 20,000 square degrees by incorporating archival DECam data from NOIRLab’s public archives¹. This release prioritizes the southern sky (Declination $\leq 32.375^\circ$), integrating new g , r , i , and z -band observations while maintaining photometric consistency across the expanded footprint. DR10 aggregates data from multiple campaigns, including the complete six-year Dark Energy Survey (DES; Dark Energy Survey Collaboration et al. 2016), the DECam Local Volume Exploration Survey (DELVE; Drlica-Wagner et al. 2021), and the DECam eROSITA Survey (DeROSITA)², with observations spanning January 2013 to August 2021. Notably, DR10 supersedes prior releases for southern sky analyses, though northern hemisphere data from BASS and MzLS remain accessible through DR9. The Legacy Surveys depths for 2 ob-

¹ <https://noirlab.edu/public/projects/astrodataarchive/>

servations at $1.5''$ seeing are predicted as $g = 24.7$, $r = 23.9$, and $z = 23.0$ mag. For additional details regarding DR10, we direct the reader to the website of the Legacy Imaging Surveys³.

2.2 Selection of cluster member stars

We applied a multi-step photometric selection. Sources were first filtered in the $(g - r)$ vs. $(g - z)$ color space using the empirical stellar locus of $g - z = 1.7 \times (g - r) - 0.17$ (Bonaca et al. 2020) with a ± 0.15 mag tolerance to accommodate photometric scatter and exclude non-stellar contaminants of galaxies and artifacts (see the left panel of Figure 1). We further refined the sample by selecting stars within $12 \leq g \leq 24.5$ to encompass the main sequence, subgiant, and red giant populations of Palomar 5, while requiring high photometric precision ($\sigma_z < 0.05$ and $\sigma_{g-r} < 0.1$). This stringent selection yielded a clean, well-measured stellar sample, optimized for subsequent analysis of the stream’s kinematic and structural properties.

We identified Palomar 5 member candidates through spatial and photometric filtering. Our selection focused on stars within a 0.5° radius circular region centered at $(\text{RA}, \text{DEC}) = (229.022^\circ, -0.112^\circ)$, covering the stream’s central area. We applied a magnitude cut of $12 \leq g \leq 24.5$ to prevent detector saturation while maintaining sufficient signal-to-noise ratio for reliable measurements. For precise color-magnitude selection as shown in the right panel of Figure 1, we implemented an extinction-corrected isochrone model with distance modulus $(m - M)_0 = 16.835$ and reddening parameters with $E(B - V) = 0.0552$ (Xu et al. 2020), using extinction coefficients $A_g = 3.214$, $A_r = 2.165$, and $A_z = 1.211$ given by Eddie Schlafly⁴. The selection envelope around the isochrone incorporated both measurement uncertainties and intrinsic dispersion, defined as $\pm(3\sigma + \sigma_{\text{intrinsic}})$. Photometric errors (σ) were determined through a robust empirical approach: stars were binned into 15 equal g-band magnitude intervals, with median errors calculated per bin and interpolated across the full magnitude range using smoothing splines. The intrinsic color dispersion was set to $\sigma_{\text{intrinsic}} = 0.03$ mag, which represents the typical intrinsic $(g - r)$ color spread of stars within a globular cluster.

3 HDBSCAN CLUSTERING ALGORITHM TO IDENTIFY CANDIDATE CLUSTER MEMBERS

3.1 HDBSCAN Algorithm Description

We identified potential member stars across the full dataset using Hierarchical Density-Based Spatial Clustering of Applications with Noise (HDBSCAN; McInnes et al. (2017)), an unsupervised clustering algorithm particularly effective for detecting structures with varying densities. This methodology leverages the strengths of both density-based clustering and distance-based classification, enabling the robust identification of member stars even in complex, low-contrast environments. Moreover, the flexibility of HDBSCAN allows it to be adapted for future searches for substructures using additional dimensions such as positional, kinematic, or CMD-based information—facilitating the discovery of finer-grained features within the stream. This capability makes it ideal for analyzing stellar populations.

³ <https://www.legacysurvey.org/dr10/description/>

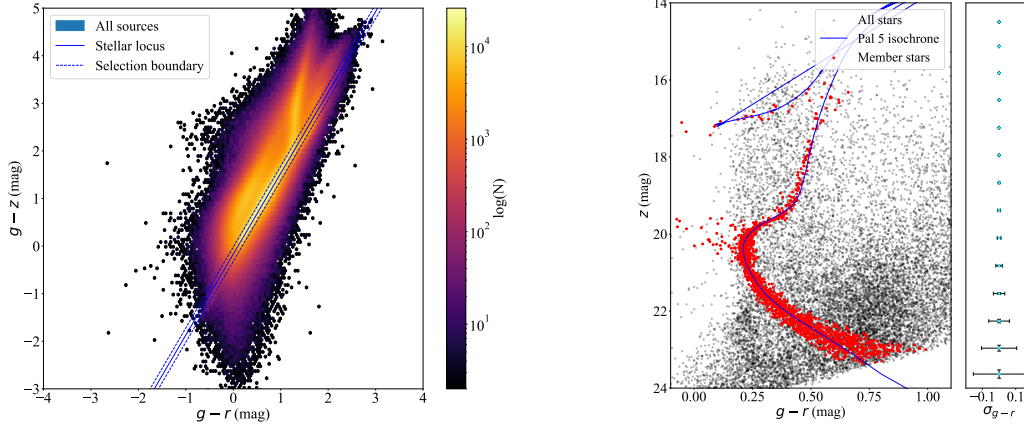


Fig. 1: Photometric selection criteria for Palomar 5 member stars. Left: Color-color diagram showing source density in $(g-r)$ vs. $(g-z)$ space, with logarithmic number density represented by the color scale. The empirical stellar locus (solid blue line) and selection boundaries (± 0.15 mag, dashed blue lines) are overplotted. Right: Color-magnitude diagram (CMD) of the central Palomar 5 region. All detected stars are shown as black points, with selected members highlighted in red circles. The blue curve represents the extinction- and distance-corrected theoretical isochrone, while error bars indicate median photometric uncertainties as a function of magnitude.

To characterize each star's photometric properties, we constructed a six-dimensional feature vector combining both magnitudes and colors. The feature vector for star i is defined as:

$$\mathbf{X}_i = [g_i, r_i, z_i, (g-r)_i, (g-z)_i, (r-z)_i], \quad (1)$$

where g_i , r_i , and z_i represent apparent magnitudes, while $(g-r)_i$, $(g-z)_i$, and $(r-z)_i$ are color indices. This combination provides complete information about each star's position in both color-magnitude and color-color space. The entire stellar sample was then represented as a feature matrix \mathbf{X} with rows corresponding to individual stars and columns to the six photometric parameters.

We implemented the HDBSCAN algorithm to identify potential members associated with the Palomar 5 stream. This approach offers significant advantages over traditional clustering methods for astronomical applications, particularly in its ability to: (i) automatically determine the optimal number of clusters without predefined parameters, (ii) effectively handle datasets with non-uniform density distributions, and (iii) robustly identify noise points in complex feature spaces. The HDBSCAN algorithm executes through two principal computational phases:

1. **Mutual Reachability Distance Calculation:** The algorithm first transforms the input feature space using a density-sensitive metric defined for any two points (p, q) as:

$$d_{\text{reach}}(p, q) = \max(\text{core_dist}(p), \text{core_dist}(q), d(p, q)), \quad (2)$$

where $d(p, q)$ represents the Euclidean distance in the six-dimensional photometric feature space, $\text{core_dist}(p)$ denotes the distance of p to its k -th nearest neighbor, serving as a proxy for local den-

2. **Cluster Extraction:** Using the mutual reachability distances, HDBSCAN constructs a minimum spanning tree and establishes a hierarchy of clusters. Clusters that prove stable across a wide range of scales are considered significant, while less stable clusters are either merged or discarded as the scale increases. Outliers are classified as noise points.

For this study, we adopted the following HDBSCAN parameters:

- **min_cluster_size = 32:** This parameter specifies the minimum number of points required to form a cluster, ensuring statistically significant overdensities are detected.
- **cluster_selection_epsilon = 0.1:** This parameter adjusts the stability threshold for cluster extraction, aiding in the isolation of well-defined structures while reducing the likelihood of spurious detections.

3.2 Membership assignment and member selection

After clustering, we assigned membership of each star based on their proximity to the cluster centers identified by HDBSCAN. For a candidate star with feature vector x , we computed its Euclidean distance to each cluster center c_j :

$$d(x, c_j) = \sqrt{\sum_{k=1}^6 (x_k - c_{j,k})^2}, \quad (3)$$

where x_k and $c_{j,k}$ denote the k -th component of the star and cluster center vectors, respectively.

A star is classified as a potential member if its distance to the nearest cluster center is below a threshold $d_{\text{threshold}}$. In our analysis, we adopted $d_{\text{threshold}} = 0.08$, based on the characteristic spread of known clusters. The resulting sample, illustrated in Figure 2, reveals the extended structure of the stream in our new LS dataset. Notably, the leading tail is now traced to $\text{DEC} \sim -15^\circ$, demonstrating a significant improvement in the characterization of the stream. The initial discovery of the Palomar 5 stream by Odenkirchen et al. (2001) and Rockosi et al. (2002) identified its leading arm only down to $\text{DEC} \sim -1.5^\circ$, while subsequent analyses, such as Bonaca et al. (2020), extended the detection limit to approximately $\text{DEC} \sim -8^\circ$. Our result therefore represents the deepest detection of the leading tail to date, offering a more complete view of the stream’s southern morphology.

4 MOCK STREAMS FOR MODELLING THE PALOMAR 5 STREAM

4.1 Galactic Potential

To generate mock streams for comparison with the observed Palomar 5 stream, the first crucial step is to select an appropriate model for the Galactic gravitational potential. While the true MW potential is inherently complex, our objective is to create a model that balances physical realism with computational efficiency. Excessive model flexibility may lead to overfitting, especially given the limited observational constraints from Palomar 5. Conversely, overly simplistic models may fail to capture key dynamical effects. Therefore, we adopt a parametric model with a minimal but adequate number of free parameters, guided by

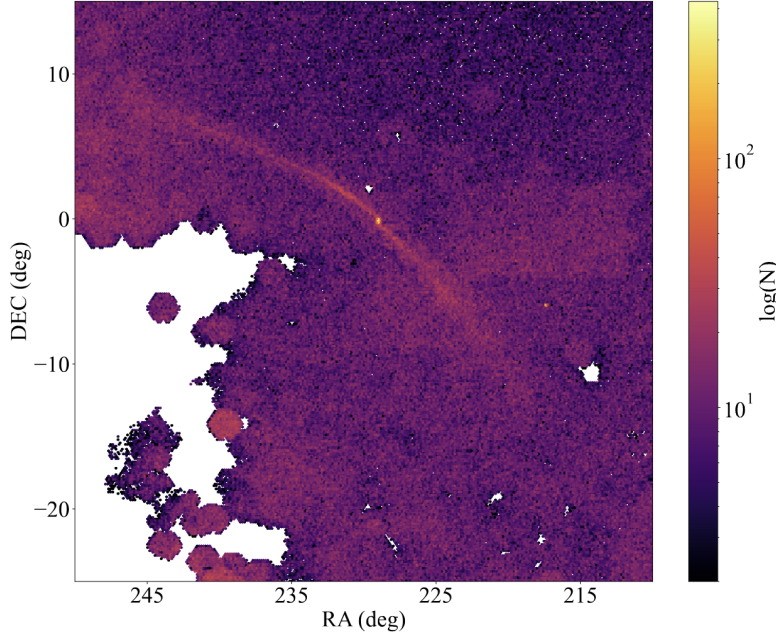


Fig. 2: Density map of sources identified as potential Palomar 5 stream members using HDBSCAN. Only sources within a normalized distance of 0.08 in feature space are included. Density is shown on a logarithmic scale, with color representing source count per bin.

Following standard practice, we decompose the MW potential into three components: a bulge, a disk, and a halo. In this work, we fix the bulge and disk parameters, while allowing flexibility only in the halo, which dominates the mass distribution at relevant Galactocentric distances for Palomar 5.

The bulge is modeled using the Hernquist potential (Hernquist 1990), which provides a spherically symmetric profile with a central cusp and finite total mass:

$$\Phi_{\text{bulge}}(r) = -\frac{GM_{\text{bulge}}}{r + a_{\text{bulge}}}, \quad (4)$$

where G is the gravitational constant, $M_{\text{bulge}} = 3.4 \times 10^{10} M_{\odot}$ is the bulge mass, $a_{\text{bulge}} = 0.7$ kpc is the scale radius, and r is the Galactocentric radial distance. The corresponding density profile is given by:

$$\rho(r) = \frac{M_{\text{bulge}}}{2\pi} \frac{a_{\text{bulge}}}{r(r + a_{\text{bulge}})^3}, \quad (5)$$

which behaves as $\rho \propto r^{-1}$ at small radii and $\rho \propto r^{-4}$ at large radii. This profile effectively captures the compact, centrally concentrated nature of the Galactic bulge.

The disk is described by the Miyamoto–Nagai potential (Miyamoto & Nagai 1975), which approximates the flattened structure of a stellar disk:

$$\Phi_{\text{disk}}(R, z) = -\frac{GM_{\text{disk}}}{\sqrt{R^2 + \left(a_{\text{disk}} + \sqrt{z^2 + b_{\text{disk}}^2}\right)^2}}, \quad (6)$$

where R and z are cylindrical coordinates, $M_{\text{disk}} = 1 \times 10^{11} M_{\odot}$ is the disk mass, and the scale parameters are $a_{\text{disk}} = 6.5$ kpc and $b_{\text{disk}} = 0.26$ kpc. This form provides a smooth transition between the bulge and

The halo, which dominates the mass distribution at large radii, is crucial for modeling tidal streams like Palomar 5. We adopt a triaxial extension of the Navarro–Frenk–White (NFW) profile (Navarro et al. 1996), which accounts for deviations from spherical symmetry. The potential is expressed by:

$$\Phi_{\text{halo}}(r_e) = -\frac{GM_{\text{halo}}}{r_e} \ln \left(1 + \frac{r_e}{r_{s,\text{halo}}} \right), \quad (7)$$

where M_{halo} is the characteristic halo mass, $r_{s,\text{halo}}$ is the scale radius and r_e is the ellipsoidal radius:

$$r_e = \sqrt{x^2 + y^2 + \frac{z^2}{q_z^2}}, \quad (8)$$

with (x, y, z) denoting Galactocentric Cartesian coordinates, and q_z being the minor-to-major axis ratios, respectively.

We treat three halo parameters— M_{halo} , $r_{s,\text{halo}}$, and q_z —as free, and fit them using stream constraints. The initial values are taken from Pearson et al. (2017), with $M_{\text{halo}} = 5 \times 10^{11} M_{\odot}$ and $r_{s,\text{halo}} = 18$ kpc. The axis ratios are initially set to $q_z = 1$, corresponding to a spherical halo, and are subsequently adjusted to explore the effects of halo shape and mass distribution on stream evolution.

4.2 Building Mock Streams

To simulate the disruption of Palomar 5 and generate its tidal stream, we employed the particle-spray method (Fardal et al. 2015) as implemented in the `Gala` package (Price-Whelan 2017). We began with Palomar 5’s present-day phase-space coordinates, integrating its orbit backward for 3 Gyr and then forward to the present in 0.5 Myr increments. At each timestep, two particles were released from the Lagrange points of the progenitor cluster. The initial positions and velocities of these particles were determined based on the distribution function described in Fardal et al. (2015), which takes into account the progenitor’s mass, size, and instantaneous orbital motion. This method effectively reproduces the formation and dynamical evolution of a tidal stream.

The progenitor’s self-gravity was modeled using a Plummer potential, and particle releases were scaled to its instantaneous tidal radius. The progenitor was initialized at its observed 6D phase-space location: $\text{RA} = 229.019^\circ$, $\text{DEC} = -0.122^\circ$, proper motions $\mu_{\alpha} \cos \delta = -2.80 \text{ mas yr}^{-1}$, $\mu_{\delta} = -2.94 \text{ mas yr}^{-1}$, a line-of-sight velocity $v_r = -57.03 \text{ km s}^{-1}$, and a heliocentric distance $d = 23.26 \text{ kpc}$ (Xu et al. 2020; Kuzma et al. 2022). These were transformed to Galactocentric coordinates, using a solar position of $R_{\odot} = 8.122 \text{ kpc}$, a solar peculiar velocity of $(U_{\odot}, V_{\odot}, W_{\odot}) = (11.1, 12.24, 7.25) \text{ km s}^{-1}$, and a circular velocity at the solar radius of $V_C = 220 \text{ km s}^{-1}$ (Schönrich et al. 2010).

We systematically varied both the progenitor and Galactic halo parameters, including the progenitor’s mass, mass-loss rate, proper motion, and distance, as well as the halo mass, scale radius, and shape parameters b and c . For each unique combination of parameters, a corresponding mock stream was generated. This suite of simulations allows us to investigate how variations in the internal properties of the progenitor and the large-scale Galactic potential influence the morphology and kinematics of the resulting stream. In particular, we seek to assess the Palomar 5’s structural sensitivity to the shape and mass distribution of the MW halo.

To ensure a comprehensive exploration of the parameter space, we produced a large number of mock

accompanied by diagnostics that characterize its properties along the stream track. These simulations provide the foundation for subsequent comparisons with the observed Palomar 5 stream and enable us to constrain both the progenitor characteristics and the Galactic potential.

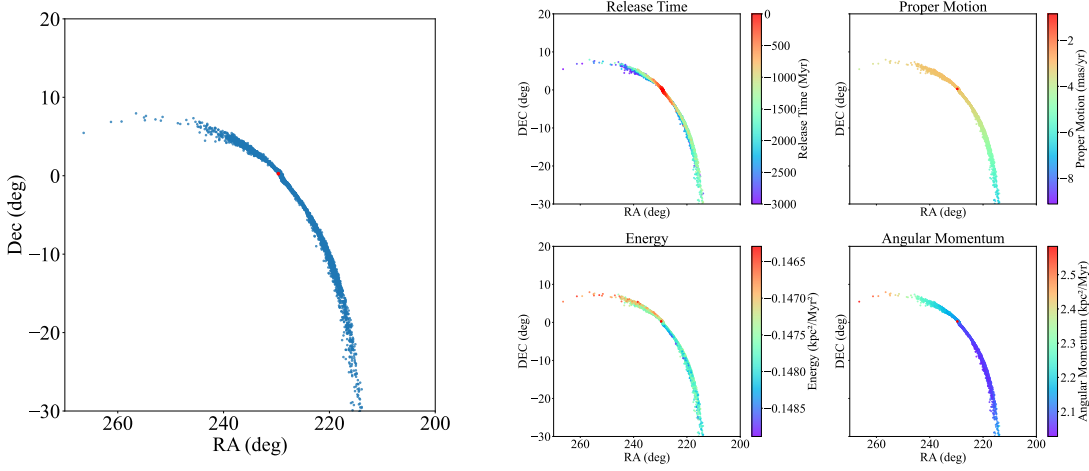


Fig. 3: Left: spatial distribution of a simulated Palomar 5 stream in the equatorial coordinate system. The progenitor is marked in red, and the stream is overlaid on the observed density map. Right: additional stream diagnostics, color-coded by (top left) release time, (top right) proper motion, (bottom left) total energy, and (bottom right) total angular momentum. The progenitor’s location is indicated by a red marker in each panel.

5 RESULTS

5.1 Extraction of the observed Palomar 5 stream

After sample selection and applying HDBSCAN, some field stars remain in the background, leading to contamination. To mitigate this, we extracted the stream’s trajectory, width, and surface density from the observed data using a Markov Chain Monte Carlo (MCMC) method. This approach models the density variations along the ϕ_2 coordinate for stars identified as potential stream members.

We model the CMD-filtered stellar density distribution along ϕ_2 (shown in the upper panel of Figure 4) using partially overlapping bins of ϕ_1 . For each bin, the density is expressed as a combination of a Gaussian component representing the Palomar 5 stream and a linearly varying background:

$$q(\phi_2) = f \mathcal{N}(\phi_2 | \mu, \sigma^2) + (1 - f)(a\phi_2 + b), \quad (9)$$

where f is the fraction of stars in the stream, $\mathcal{N}(\phi_2 | \mu, \sigma^2)$ is the Gaussian distribution with mean μ (the stream centroid) and standard deviation σ (the stream width), and a and b are the parameters of the linear background. The likelihood function is defined as:

$$\ln \mathcal{L}(\theta) = \sum_i \ln q(\phi_{2,i} | f, \mu, \sigma, a, b), \quad (10)$$

We implement the MCMC sampler using the `emcee` package to generate posterior samples $p(\theta|\phi_2) \propto \mathcal{L}(\theta)p(\theta)$ for each ϕ_1 bin. The walkers are initialized with small Gaussian perturbations around $\theta_0 = (0.2, 0.1, 0.05, 0, 1)$, with an initial perturbation scale $\sigma_{\text{init}} = 10^{-1}$. Figure 4 presents the results of the MCMC fitting applied to the observational data. The extracted stream parameters form a basis for comparing the observed stream to simulated mock streams.

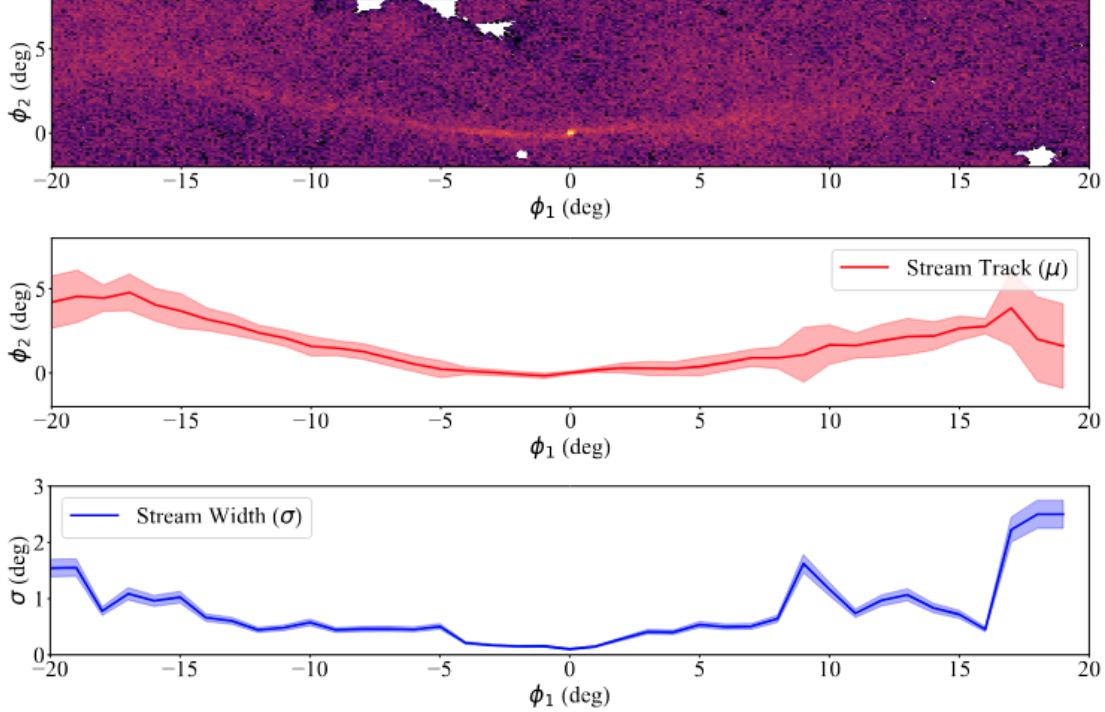


Fig. 4: Visualization of the Palomar 5 tidal stream in the transformed coordinate system. Top panel: spatial distribution of the stream in the ϕ_1 - ϕ_2 coordinate system, with density color-coded on a logarithmic scale. Middle panel: stream track (μ) along ϕ_1 estimated through MCMC fitting, with a shaded region representing the uncertainty ($\pm\sigma$) in the stream's location along ϕ_2 . Bottom panel: stream width (σ) along ϕ_1 , with a shaded region indicating the 16th and 84th percentile confidence intervals.

To evaluate the dynamical model of the Palomar 5 stream, we compare the observed stream properties with simulated mock streams generated by the `MockStreamGenerator` from the `Gala` package. These mock streams are produced by integrating the progenitor orbit in a static potential that includes a Hernquist bulge, a Miyamoto-Nagai disk, and an eNFW halo. The mock streams are then transformed into the ϕ_1 - ϕ_2 coordinate system for comparison.

To quantify the agreement between the observed and mock streams, we extract the track of the mock stream in the same manner as the observed stream. This involves binning the mock stream particles along ϕ_1 , fitting a Gaussian to the ϕ_2 distribution in each bin, and obtaining the track and width. Residuals are then computed by comparing the track positions and widths:

$$d_{\text{residual}}(\phi_1) = \frac{(\mu_{\text{obs}}(\phi_1) - \mu_{\text{mock}}(\phi_1))^2}{\sigma_{\text{obs}}^2(\phi_1) + \sigma_{\text{mock}}^2(\phi_1)}, \quad (11)$$

where $\mu_{\text{obs}}(\phi_1)$ and $\mu_{\text{mock}}(\phi_1)$ are the observed and mock stream track positions, and $\sigma_{\text{obs}}(\phi_1)$ and

squared residuals:

$$\ln \mathcal{L}(\theta) = -\frac{1}{2} \sum_i [d_{\text{residual},i}^2]. \quad (12)$$

5.2 Best-fit model by matching with the observed stream

In this section, we present the results of our efforts to identify the best-fit stream by comparing the observed Palomar 5 stream with a large set of mock streams generated under varying Galactic potential and stream parameters. This comparison allows us to determine the optimal combination of Galactic halo and stream parameters that best matches the observed data. We performed a joint MCMC analysis to simultaneously constrain both the Galactic potential parameters and the stream parameters. The MCMC process involves varying eight parameters: three associated with the Galactic halo (M_{halo} , $r_{s,\text{halo}}$, and q_z) and five related to the Palomar 5 properties (M_{gc} , dM_{gc}/dt , $\mu_\alpha \cos \delta$, μ_δ , and D). While these Palomar 5 parameters are treated as free in our model to ensure self-consistency, some of them (such as the proper motion and distance) are already relatively well constrained from previous work. Including them in the fit allows us to validate the consistency of our model with independent measurements. As a consequence, the posterior distributions of these well-measured parameters are notably narrow and closely aligned with the external constraints (Figure 5).

The results of the MCMC sampling are visualized in Figure 5, which displays a corner plot illustrating the marginalized posterior distributions of the eight parameters. The constraints imposed by the observed stream track are evident, with the tightest constraints found for the Palomar 5 globular cluster’s mass (M_{gc}) and proper motions ($\mu_\alpha \cos \delta$ and μ_δ). In contrast, the distribution of Galactic halo parameters are relatively broader, reflecting their more complex relationship with the morphology of the stream.

Using the best-fit parameters obtained from the MCMC analysis ($M_{\text{halo}} = 5.67 \times 10^{11} M_\odot$, $r_{s,\text{halo}} = 28.94$ kpc, $q_z = 0.93$, $M_{\text{gc}} = 4.31 \times 10^3 M_\odot$, $dM_{\text{gc}}/dt = 1.81 M_\odot \text{ Myr}^{-1}$, $\mu_\alpha \cos \delta = -2.28 \text{ mas yr}^{-1}$, $\mu_\delta = -2.26 \text{ mas yr}^{-1}$, and $D = 23.25$ kpc), we generate a mock stream that matches the observed data. Figure 6 presents the best-fit mock stream, which is directly compared to the observed data. The simulated stream closely follows the observed stream track, with minimal residuals between the mock stream particles and the spline-interpolated observed stream. The alignment is particularly pronounced along the main body of the stream, where the density and morphology of the simulated stream closely correspond to the observed features. This indicates that the Galactic potential model and stream parameters derived from the MCMC analysis accurately capture the dynamics of the observed Palomar 5 stream.

In addition to the visual agreement, the stream’s width and density profile are also well reproduced by the best-fit mock stream. The stream width, as derived from the MCMC fitting, closely matches the observed spread of stars in the ϕ_2 coordinate, further validating the reliability of the best-fit parameters. The best-fit mock stream not only accurately replicates the observed stream track but also captures key features of the stream’s morphology, density, and kinematics. This strongly supports the notion that the chosen Galactic potential and stream model accurately describe the dynamics of the Palomar 5 stream. These results highlight the potential of tidal streams as probes of the Galactic potential. Future improvements, such as including time-varying perturbations or exploring alternative halo density profiles, could enhance

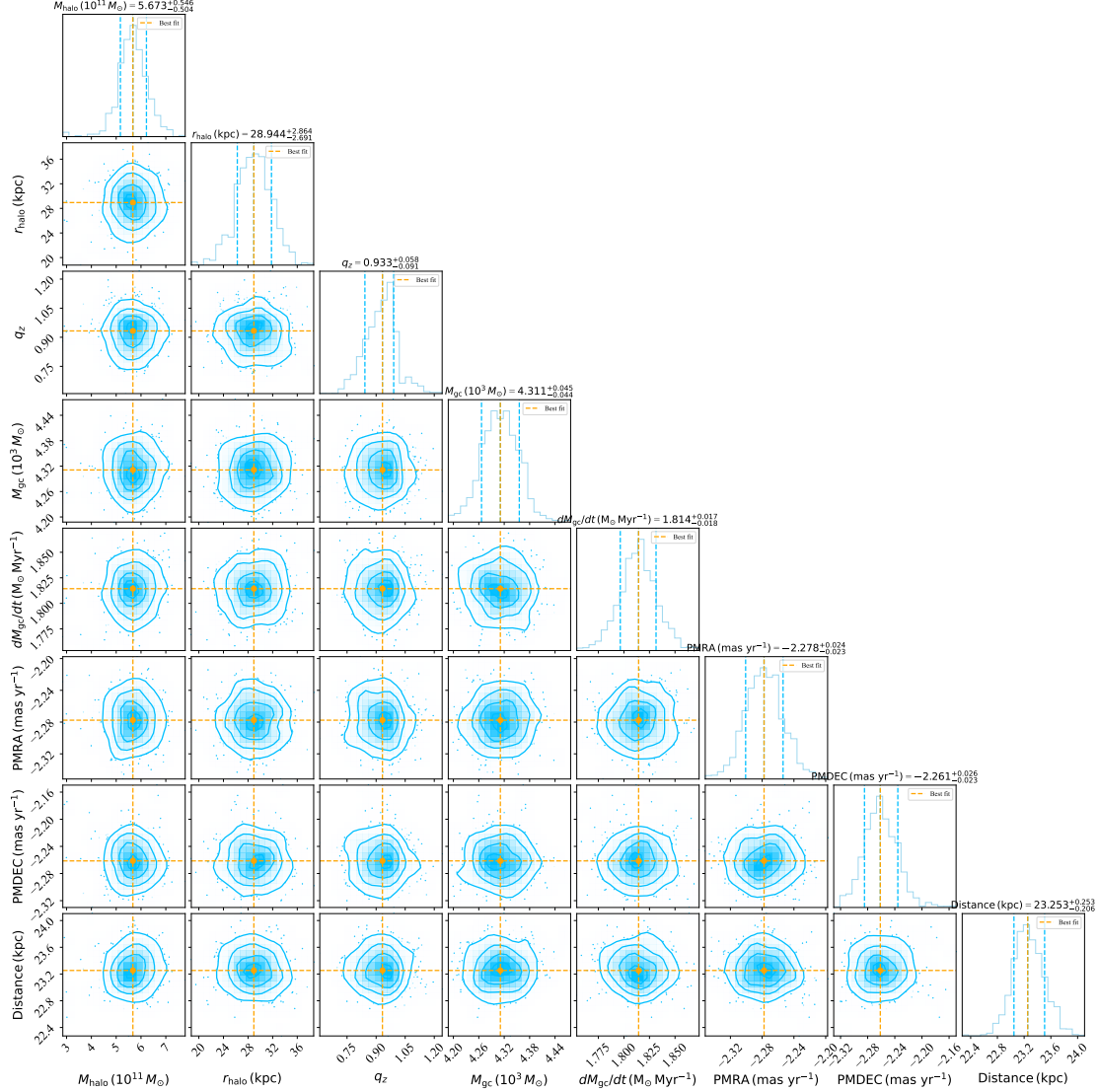


Fig. 5: Corner plot of the MCMC sampling results for the halo and stream parameters. This plot displays the marginalized posterior distributions and pairwise correlations for the eight parameters: M_{halo} , $r_{s,\text{halo}}$, q_z , M_{gc} , dM_{gc}/dt , $\mu_\alpha \cos \delta$, μ_δ , and D . The orange dashed lines indicate the median values for each parameter, while the blue dashed lines represent the 16th and 84th percentile values.

5.3 Comparing q_z with other studies and some discussions

We now contextualize our results within the framework of previous studies that have constrained the shape of the MW's dark matter halo using various observational probes, including different stellar streams and Cepheids (Huang et al. 2024). As shown in Fig. 7, our estimate of the halo flattening aligns well with those reported in the literature reinforcing the emerging view of a nearly spherical or mildly flattened Galactic potential within the radial range explored by these tracers.

Among the most directly comparable studies are those analyzing other stellar streams at similar Galactocentric distances. Although the specific regions of the halo probed differ in orientation, vertical

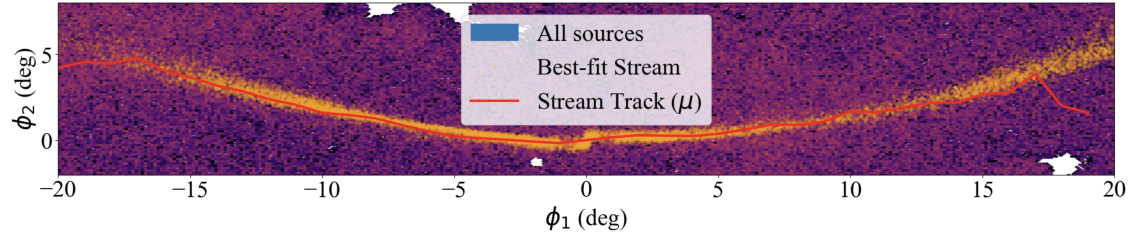


Fig. 6: Distribution of the best-fit mock stream. The hexbin plot illustrates the distribution of all sources, with the color indicating the logarithmic density of sources. The orange points represent the best-fit stream, while the red line denotes the observation stream track derived from the MCMC fitting.

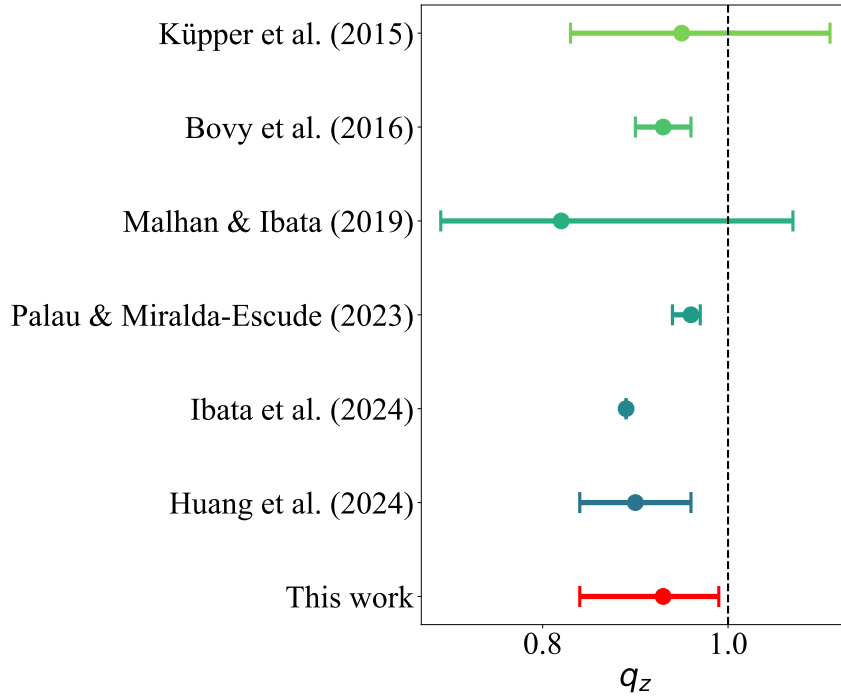


Fig. 7: q_z values for various studies. Each point with an error bar represents a different study, while the red point corresponds to our work. Horizontal error bars show the measurement uncertainties and a vertical dashed line at $q_z = 1$ is included for reference. The studies are listed chronologically along the y-axis.

uncertainties. Our results fall within this general distribution, further reinforcing the reliability of stream-based constraints on the dark matter halo shape.

Several studies, such as those by Bovy et al. (2016) and Küpper & et al. (2015), have focused on well-known streams like GD-1 and Palomar 5, whose distinct morphologies and extensive coverage across the sky make them sensitive to the global potential. Despite differing methodologies, including orbit fitting, action-angle modeling, and full N -body simulations, these studies arrive at values of q_z that are largely compatible with our findings.

Recent analyses have built upon this foundation by incorporating *Gaia* data and modern statistical techniques to examine additional streams or stellar populations. For instance, Malhan & Ibata

track modeling, or mock-stream generation in realistic potentials to further refine estimates of the halo’s flattening. Although some of these studies suggest slightly oblate or prolate halos depending on the tracer population and radial regime, they collectively rule out extreme deviations from sphericity, a conclusion consistent with our result. In particular, our estimate lies well within the 1σ range of most previous constraints, while providing a tighter uncertainty due to the well-constrained and more extensive stream track with a larger number of stars. The agreement of our result with those derived from independent tracers and methods offers compelling evidence for a dark matter halo that is close to spherical in the region between ~ 10 and 20 kpc from the Galactic center.

6 CONCLUSION

In this work, we present a comprehensive analysis of the Palomar 5 tidal stream using data from the DESI LS DR10. By applying the HDBSCAN clustering algorithm, we significantly extended the known extent of the stream, tracing its leading tail down to $\delta \sim -15^\circ$, an area poorly constrained in earlier studies. This advancement provides a more complete view of the stream’s morphology, particularly in the outer regions, and highlights the effectiveness of combining deep imaging surveys with advanced clustering techniques to uncover faint tidal features.

We conducted a detailed comparison between the observed stream and mock streams generated under various Galactic halo models. The best-fit simulation matches the observed stream track and width closely, indicating that our inferred parameters for the MW potential and the stream progenitor provide a reliable dynamical description. These findings confirm the sensitivity of the Palomar 5 stream to the underlying gravitational potential, and demonstrate the utility of stellar streams as precise probes of the Galactic halo structure.

Our modeling places meaningful constraints on the shape, mass, and scale radius of the MW dark matter halo, with results that align broadly with previous studies that used other streams and Cepheids. The success of our approach illustrates the power of combining observational data with realistic stream modeling to disentangle the structure of the dark halo. While our model assumes a static Galactic potential, future refinements could incorporate time-dependent effects or alternative halo profiles to explore potential interactions between the stream and halo substructures.

Looking ahead, our study highlights the value of deep imaging surveys and clustering-based analyses in identifying and characterizing faint tidal debris. The growing availability of wide-field datasets from ongoing and upcoming surveys, such as the Wide Field Survey Telescope (WFST; Wang et al. 2023), Large Synoptic Survey Telescope (LSST; Ivezić et al. 2019), China Space Station Telescope (CSST; Zhan 2011, 2021) and Wide-Field InfraRed Survey Telescope (WFIRST; Akesson et al. 2019), will facilitate the detection of even subtler structures in the outer halo. Continued development of simulation frameworks and data-driven methods will further enhance our understanding of the MW’s dynamical history and the distribution of its dark matter component.

Acknowledgements The work is supported by the National Key R&D Program of China (grant Nos. 2023YFA1607800, 2023YFA1607804, 2022YFA1602902, 2023YFA1608100), the National Natural

The authors also acknowledge the science research grants from the China Manned Space Project and the Strategic Priority Research Program of the Chinese Academy of Sciences with Grant Nos. XDB0550100 and XDB0550000.

References

- Akeson, R., Armus, L., Bachelet, E., et al. 2019, arXiv e-prints, arXiv:1902.05569 14
- Amorisco, N. C., & Evans, N. W. 2016, *Monthly Notices of the Royal Astronomical Society*, 461, 1144 1
- Amorisco, N. C., Gómez, F. A., Vegetti, S., & White, S. D. 2016, *Monthly Notices of the Royal Astronomical Society: Letters*, 463, L17 2
- Banik, N., & Bovy, J. 2019, *Monthly Notices of the Royal Astronomical Society*, 484, 2009 1
- Bernard, E. J., & et al. 2016, *The Astrophysical Journal*, 818, 31 2
- Blum, R. D., Burleigh, K., Dey, A., et al. 2016, in *American Astronomical Society Meeting Abstracts*, Vol. 228, American Astronomical Society Meeting Abstracts #228, 317.01 3
- Bode, P., & et al. 2001, *The Astrophysical Journal*, 556, 93 2
- Bonaca, A., & Hogg, D. W. 2018, *The Astrophysical Journal*, 867, 101 2
- Bonaca, A., Hogg, D. W., Price-Whelan, A. M., & Conroy, C. 2019, *The Astrophysical Journal*, 880, 38 2
- Bonaca, A., & Price-Whelan, A. M. 2024, *New Astronomy Reviews*, 101713 2
- Bonaca, A., Pearson, S., Price-Whelan, A. M., et al. 2020, *The Astrophysical Journal*, 889, 70 2, 4, 6
- Bovy, J., Bahmanyar, A., Fritz, T. K., & Kallivayalil, N. 2016, *The Astrophysical Journal*, 833, 31 13
- Bovy, J., & Rix, H. W. 2016, *Annual Review of Astronomy and Astrophysics*, 54, 45 2
- Carlberg, R. G., & et al. 2012, *The Astrophysical Journal*, 746, 88 2
- Dark Energy Survey Collaboration, Abbott, T., Abdalla, F. B., et al. 2016, *MNRAS*, 460, 1270 3
- DESI Collaboration, Aghamousa, A., Aguilar, J., et al. 2016, arXiv e-prints, arXiv:1611.00036 3
- Dey, A., Schlegel, D. J., Lang, D., et al. 2019, *AJ*, 157, 168 3
- Drlica-Wagner, A., Carlin, J. L., Nidever, D. L., et al. 2021, *ApJS*, 256, 2 3
- Erkal, D., & et al. 2017, *Monthly Notices of the Royal Astronomical Society*, 470, 4769 2
- Fardal, M. A., Huang, S., & Weinberg, M. D. 2015, *MNRAS*, 452, 301 8
- Hernquist, L. 1990, *ApJ*, 356, 359 7
- Huang, Y., Feng, Q., Khachaturyants, T., et al. 2024, *Nature Astronomy*, 8, 1294 12
- Ibata, R. A., & et al. 2016, *The Astrophysical Journal*, 819, 27 2
- Ibata, R., Malhan, K., Tenachi, W., et al. 2024, *The Astrophysical Journal*, 967, 89 2, 13
- Ivezić, Ž., Kahn, S. M., Tyson, J. A., et al. 2019, *The Astrophysical Journal*, 873, 111 14
- Koposov, S. E., & et al. 2010, *The Astrophysical Journal*, 717, 1084 2
- Kroupa, P. 2015, *Physics Reports*, 568, 1 2
- Kuzma, P. B., Ferguson, A., Varri, A. L., et al. 2022, *Monthly Notices of the Royal Astronomical Society*, 512, 315 8
- Küpper, A. H. W., & et al. 2015, *Monthly Notices of the Royal Astronomical Society*, 451, 4110 2, 13
- Mainzer, A., Bauer, J., Cutri, R. M., et al. 2014, *ApJ*, 792, 30 3

- McInnes, L., Healy, J., Astels, S., et al. 2017, *J. Open Source Softw.*, 2, 205 4
- Milgrom, M. 1983, *The Astrophysical Journal*, 270, 365 2
- Miyamoto, M., & Nagai, R. 1975, *PASJ*, 27, 533 7
- Navarro, J. F., Frenk, C. S., & White, S. D. M. 1996, *ApJ*, 462, 563 8
- Odenkirchen, M., & et al. 2001, *The Astrophysical Journal*, 548, L165 2
- Odenkirchen, M., Grebel, E. K., Rockosi, C. M., et al. 2001, *The Astrophysical Journal*, 548, L165 6
- Palau, C. G., & Miralda-Escudé, J. 2023, *Monthly Notices of the Royal Astronomical Society*, 524, 2124 13
- Pearson, M. J., & D’Onghia, E. 2017, *The Astrophysical Journal*, 849, 56 1, 2
- Pearson, S., Küpper, A. H., Johnston, K. V., & Price-Whelan, A. M. 2015, *The Astrophysical Journal*, 799, 28 2
- Pearson, S., Price-Whelan, A. M., & Johnston, K. V. 2017, *Nature Astronomy*, 1, 633 8
- Price-Whelan, A. M. 2017, *The Journal of Open Source Software*, 2, 388 8
- Price-Whelan, A. M., & Bonaca, A. 2018, *The Astrophysical Journal*, 862, 4 2
- Rockosi, C. M., & et al. 2002, *The Astronomical Journal*, 123, 1926 2
- Rockosi, C. M., Odenkirchen, M., Grebel, E. K., et al. 2002, *The Astronomical Journal*, 124, 349 6
- Schönrich, R., Binney, J., & Dehnen, W. 2010, *Monthly Notices of the Royal Astronomical Society*, 403, 1829 8
- Silva, D. R., Blum, R. D., Allen, L., et al. 2016, in *American Astronomical Society Meeting Abstracts*, Vol. 228, *American Astronomical Society Meeting Abstracts #228*, 317.02 3
- Starkman, N., Nibauer, J., Bovy, J., et al. 2025, *The Astrophysical Journal*, 980, 253 2
- Thomas, G., & et al. 2016, *Monthly Notices of the Royal Astronomical Society*, 459, 4575 2
- Wang, T., Liu, G., Cai, Z., et al. 2023, *Science China Physics, Mechanics & Astronomy*, 66, 109512 14
- Wright, E. L., Eisenhardt, P. R. M., Mainzer, A. K., et al. 2010, *AJ*, 140, 1868 3
- Xu, X., Zou, H., Zhou, X., et al. 2020, *The Astronomical Journal*, 161, 12 4, 8
- Zhan, H. 2011, *Scientia Sinica Physica, Mechanica & Astronomica*, 41, 1441 14
- Zhan, H. 2021, *Chinese Science Bulletin (Chinese Version)*, 66, 1290 14
- Zou, H., Zhou, X., Fan, X., et al. 2017, *PASP*, 129, 064101 3